



[Rb/Zr] ratio in Ba stars as a diagnostic of the companion AGB stellar mass

J. SHEJEELAMMAL*  and ARUNA GOSWAMI*

Indian Institute of Astrophysics, Sarjapur Road, Koramangala, Bengaluru 560 034, India.

*Corresponding author. E-mail: shejeelammal.j@iiap.res.in; aruna@iiap.res.in

MS received 30 August 2020; accepted 17 September 2020

Abstract. Understanding nucleosynthesis in and evolution of asymptotic giant branch (AGB) stars is of primary importance as these stars are the main producers of some of the key elements in the Universe. They are the predominant sites for slow-neutron-capture nucleosynthesis (s-process). The exact physical conditions and nucleosynthetic processes occurring in the interior of AGB stars are not clearly understood, and that hinders better understanding of the contribution of these stars to the Galactic chemical enrichment. Extrinsic-variable stars that are known to have received products of AGB phase of evolution via binary mass-transfer mechanisms are vital tools in tracing AGB nucleosynthesis. The [Rb/Zr] ratio is an important diagnostic to understand the average neutron density at the s-process site and provides important clues to the mass of companion AGB stars in binaries. In this work we have presented estimates of [Rb/Zr] ratios based on high-resolution spectroscopic analysis for a sample of Ba stars, and discussed how the ratio can be used to understand the characteristics of the AGB star. Results from an analysis based on a parametric model to confirm the mass of the companion AGB star are also presented.

Keywords. Stars—abundance—stars—chemically peculiar—stars—nucleosynthesis.

1. Introduction

Barium (Ba II) stars are peculiar G and K type stars which were first identified by Bidelman and Keenan (1951). Their surface chemical composition is characterized by overabundance of elements heavier than iron and $C/O < 1$ (Barbuy *et al.* 1992; Allen and Barbuy 2006; Drake and Pereira 2008; Pereira and Drake 2009). They exhibit abnormally strong lines of s-process (slow-neutron-capture process) elements such as Ba II at λ 4554 Å, Sr II at λ 4077 Å, as well as enhanced CH, CN and C_2 molecular bands. They are mostly in their main-sequence and giant phase of stellar evolution. Nucleosynthesis theories do not support occurrence of heavy-element nucleosynthesis during the stellar evolutionary phases to which these stars belong.

It is known that asymptotic giant branch (AGB) stars are the major producers of s-process elements in

the Universe (Busso *et al.* 1999). The s-process-enriched materials produced in the interiors of AGB stars are brought to the surface through a third dredge-up (TDU) process. The observed overabundance of heavy elements at the surface of Ba stars could not be attributed to an intrinsic origin as they are not luminous enough to undergo s-process nucleosynthesis. This posed a challenge to existing nucleosynthesis theories.

Radial velocity monitoring studies of Ba stars have shown that 85% of Ba stars are in binaries (McClure *et al.* 1980; McClure 1983, 1984; McClure and Woodsworth 1990; Udry *et al.* 1998a, b; Lucatello *et al.* 2005) with a now-invisible white dwarf companion. Later studies confirmed that all giant Ba stars are binaries (Jorissen *et al.* 2019). A generally accepted scenario that explains the observed high abundances of neutron-capture elements is a binary mass transfer picture. These stars are believed to have received via binary mass-transfer mechanisms products of the companion stars produced during their AGB phase of evolution. Hence, the chemical composition of this class of objects can be used to trace the AGB nucleosynthesis at their corresponding metallicity.

Detailed chemical composition studies of AGB stars can provide better understanding of the evolution of heavy elements in the Galaxy. The molecular contribution dominant spectra of AGB stars make the derivation of exact elemental abundance difficult. In this regard, the spectra of the comparatively warmer, extrinsically s-process-enhanced Ba stars could make the derivation of elemental abundance much easier and help probe s-process enrichment of the Galaxy.

Several aspects of Ba stars, such as mass, abundance peculiarities, kinematics, etc., have been extensively studied by many workers (Allen and Barbay 2006; Smiljanic *et al.* 2007; de Castro *et al.* 2016; Mahanta *et al.* 2016; Yang *et al.* 2016; Karinkuzhi *et al.* 2018; Purandardas *et al.* 2019; Shejellammal *et al.* 2020 and references therein). In addition to probing of s-process enrichment of the Galaxy, surface chemical composition analysis of Ba stars could also be used to characterize the initial mass of the companion AGB stars. Mass is one of the important basic parameters of stars; the neutron source and nucleosynthesis product distribution varies with initial stellar mass. In case of AGB stars, there are two important neutron sources for the s-process in the He intershell: $^{13}\text{C}(\alpha, n)^{16}\text{O}$ reaction during the radiative inter-pulse period, and $^{22}\text{Ne}(\alpha, n)^{25}\text{Mg}$ reaction during the convective thermal pulses (TP). $^{13}\text{C}(\alpha, n)^{16}\text{O}$ reaction is the dominant neutron source in low-mass AGB stars with initial mass $\leq 3 M_{\odot}$. The temperature required for the operation of this reaction is $T \geq 90 \times 10^6$ K and provides a neutron density N_n of $\sim 10^8 \text{ cm}^{-3}$ in a timescale of $\geq 10^3$ years (Straniero *et al.* 1995; Gallino *et al.* 1998; Goriely and Mowlavi 2000; Busso *et al.* 2001). The temperature required for the activation of ^{22}Ne source is 300×10^6 K, which is achieved during TP in intermediate-mass AGB stars (initial mass $\geq 4 M_{\odot}$). It produces a neutron density N_n of $\sim 10^{13} \text{ cm}^{-3}$ in a timescale of ~ 10 years. The temperature required for the ^{22}Ne source is reached in low-mass stars during the last few TP providing N_n of $\sim 10^{10} - 10^{11} \text{ cm}^{-3}$ (Iben 1975; Busso *et al.* 2001).

Rb plays a unique role as a diagnostic of neutron density at the s-process site. Rb is the only low-neutron-density branch available to stellar spectroscopists as a neutron densitometer (Tomkin and Lambert 1999). Rb is produced only when $N_n > 5 \times 10^8 \text{ cm}^{-3}$, otherwise Sr, Y, Zr, etc. are produced. Hence, [Rb/Zr] ratio can be used as an indicator of mass of AGB stars. Theoretical models predict a negative value for [Rb/

Zr] ratio in low-mass AGB stars and a positive value in intermediate-mass AGB stars (Abia *et al.* 2001; Karakas *et al.* 2012; van Raai *et al.* 2012). We have used the neutron-density-dependent [Rb/Zr] ratio in a sample of barium stars to infer mass of companion AGB stars. Such studies are scanty in the literature.

In this work, we present results obtained from a detailed chemical composition analysis of four Ba stars, HD 32712, HD 36650, HD 179832 and HD 211173, based on high-resolution, high-quality spectra. We have determined the abundances of heavy elements such as Rb, Sr, Y, Zr, Ba, La, Ce, Pr, Nd, Sm and Eu in these stars. The details of the spectra, abundance analysis and the interpretations of the results are discussed in the subsequent sections.

2. Data acquisition and data reduction

The objects analysed in this study were taken from the barium star catalog of Lü (1991). High-resolution ($\lambda/\delta\lambda \sim 48,000$) FEROS (Fiber-fed Extended Range Optical Spectrograph attached to the 1.52 m telescope of ESO at La Silla, Chile) spectra were used for all the four objects. The wavelength coverage spans 3520–9200 Å. Data reduction was performed using the basic tasks in Image Reduction and Analysis Facility (IRAF) software. A few sample spectra are shown in Figure 1.

3. Data analysis

3.1 Determination of stellar atmospheric parameters

Data analysis was performed using the most recent version of the radiative transfer code MOOG (Snedden 1973) based on the assumptions of local thermodynamic equilibrium (LTE). The stellar atmospheric parameters, the effective temperature T_{eff} , the surface gravity $\log g$, micro-turbulent velocity ζ and the metallicity [Fe/H] were determined using a set of clean, unblended Fe I and Fe II lines with excitation potential in the range 0.0–6.0 eV and equivalent width 20–180 mÅ. An initial model atmosphere was selected from the Kurucz grid of model atmosphere with no convective overshooting (<http://cfaku5.cfa.harvard.edu/>) using the photometric temperature estimate and the initial guess of $\log g$ value for giants/dwarfs. The final model atmosphere was obtained through an iterative method from the initially selected one. The

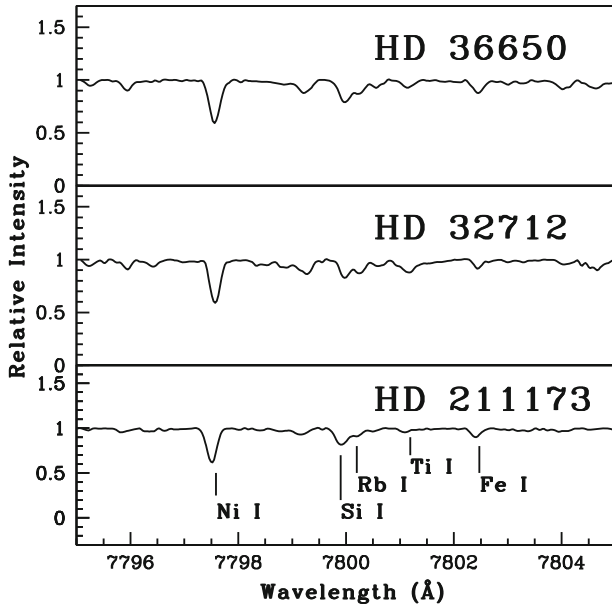


Figure 1. Sample spectra of the program stars in the wavelength region 7795 to 7805 Å.

effective temperature was determined by forcing the slope of abundances versus excitation potential of the measured Fe I lines to zero. The micro-turbulent velocity at that particular temperature was fixed to be that value for which there is no dependence of the abundances derived from the Fe I lines on the reduced equivalent width. The surface gravity was obtained by demanding that the abundances derived from both Fe I and Fe II lines give nearly the same values at the selected effective temperature and micro-turbulent velocity. The abundances obtained from the Fe I and Fe II lines give the metallicity. With this finally adopted model atmosphere, further abundance analysis was carried out.

3.2 Abundances of heavy elements

The abundance of Rb is derived using the spectral synthesis calculation of Rb I resonance line at 7800.259 Å (Figure 2). We could not detect the Rb I lines in the warmer program stars. The Rb I resonance line at 7947.597 Å is not usable for the abundance estimation. The hyper-fine components of Rb were taken from Lambert and Luck (1976). The Sr abundance was derived from the spectral synthesis calculation of Sr I line at 4607.327 Å. The Y I line at 6435.004 Å was used to derive the Y I abundances, while Y II abundances were derived from the measured equivalent width of several Y II lines. We have

derived the Zr abundance from the spectral synthesis of Zr I line at 6134.585 Å (Figure 3) and from the equivalent width measurement of several Zr II lines. The abundances of Ba and La are derived from the spectral synthesis calculation of Ba II line at 5853.668 Å and La II line at 4921.776 Å. The hyper-fine components of Ba were taken from McWilliam (1998) and those of La from Jonsell *et al.* (2006). To derive the abundances of elements Ce, Pr, Nd and Sm, equivalent width measurement of several singly ionized lines were used. The Eu abundances are derived from the spectral synthesis calculation of Eu II line at 6645.064 Å by considering the hyper-fine components from Worely *et al.* (2013).

4. Results and discussion

4.1 [Rb/Zr] ratio as a diagnostic of the neutron density at the s-process site

Rb is an s-process element produced from neutron capture by ^{84}Kr . The s-process path going through Rb is shown in Figure 4. The branching points at the unstable nuclei ^{85}Kr and ^{86}Rb control Rb production along the s-process nucleosynthesis path through Rb. The probability of these unstable nuclei capturing a neutron before β -decaying determines the amount of Rb produced, which in turn depends on the neutron density at the s-process site (Tomkin and Lambert 1983; Beer and Macklin 1989; Lambert *et al.* 1995). When ^{84}Kr undergoes neutron capture, 50% of the flux goes to the ground state of ^{85}Kr and the other 50% goes to the metastable state of ^{85}Kr . Out of this metastable ^{85}Kr , 80% decays to ^{85}Rb , while the remaining 20% decays to its ground state. In effect, 40% of the $^{84}\text{Kr}+n$ produces ^{85}Rb , whereas the remaining 60% results in the production of ground state ^{85}Kr . At higher neutron densities, $N_n > 5 \times 10^8 \text{ n/cm}^3$, the long-lived ^{85}Kr ($t_{1/2} \sim 10.75 \text{ yr}$) undergoes neutron capture allowing the reaction $^{85}\text{Kr}(n, \gamma)^{86}\text{Kr}(n, \gamma)^{87}\text{Kr}$. The short-lived ^{87}Kr ($t_{1/2} \sim 76.3 \text{ min}$) decays quickly to the stable ^{87}Rb . The other unstable isotope ^{86}Rb ($t_{1/2} \sim 18.63 \text{ days}$), which is produced by neutron capture by ^{85}Rb , directly produces ^{87}Rb provided the neutron density is $\geq 10^{10} \text{ n/cm}^3$. At lower neutron densities, ^{86}Rb decays to ^{86}Sr allowing for $^{86}\text{Sr}(n, \gamma)^{87}\text{Sr}(n, \gamma)^{88}\text{Sr}$ (Beer 1991; Lugaro and Chieffi 2011).

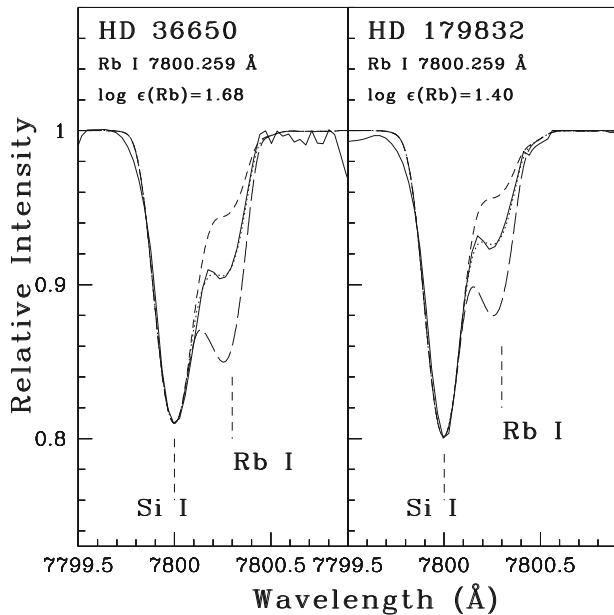


Figure 2. Synthesis of Rb I line around 7800 Å. The dotted line represents synthesized spectra and the solid line indicates the observed spectra. The short-dash line represents the synthetic spectra corresponding to $\Delta[\text{Rb}/\text{Fe}] = -0.3$ and the long-dash line corresponds to $\Delta[\text{Rb}/\text{Fe}] = +0.3$.

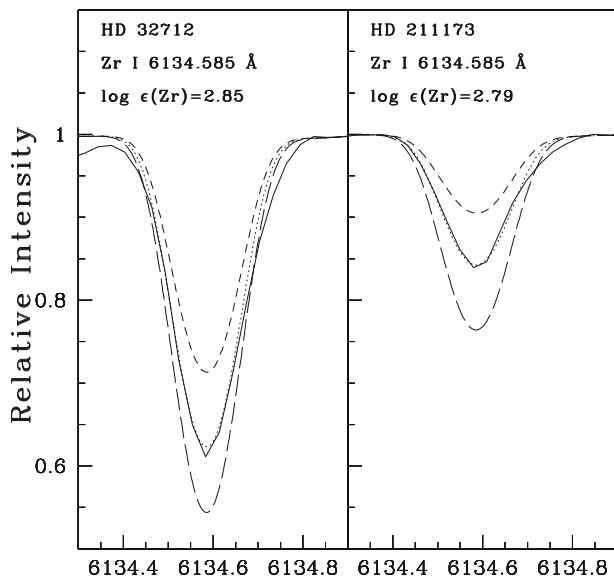


Figure 3. Synthesis of Zr I line at 6134.585 Å. The dotted line represents synthesized spectra and the solid line indicates the observed spectra. The short-dash line represents the synthetic spectra corresponding to $\Delta[\text{Zr}/\text{Fe}] = -0.3$ and the long-dash line corresponds to $\Delta[\text{Zr}/\text{Fe}] = +0.3$.

The magic number of neutrons of ^{87}Rb makes it stable against neutron capture. The smaller neutron-capture cross-section of ^{87}Rb ($\sigma \sim 15.7$ mbarn at 30

keV) compared to that of ^{85}Rb ($\sigma \sim 234$ mbarn) (Heil *et al.* 2008) favours the accumulation of ^{87}Rb once it is formed. Therefore, the isotopic ratio $^{87}\text{Rb}/^{85}\text{Rb}$ could be a direct indicator of the neutron density at the s-process site, which in turn helps to infer the mass of the AGB star. But it is impossible to distinguish the lines due to these two isotopes of Rb in stellar spectra (Lambert and Luck 1976; García-Hernández *et al.* 2006). However, the abundance of Rb relative to other elements in this region of the s-process path, such as Sr, Y and Zr, can be used to estimate the average neutron density of the s-process. Both the theoretical models and the observations have shown that the $[\text{Rb}/\text{Zr}]$ ratio has a negative value in AGB stars with $M < 3M_{\odot}$ and a positive value in massive AGB stars with mass $M > 3M_{\odot}$ (Plez *et al.* 1993; Lambert *et al.* 1995; Abia *et al.* 2001; García-Hernández *et al.* 2006, 2007, 2009; Karakas *et al.* 2012; van Raai *et al.* 2012).

We could derive the $[\text{Rb}/\text{Zr}]$ ratio in all the four Ba stars; the estimated values are given in Table 1. The observed $[\text{Rb}/\text{Fe}]$ and $[\text{Zr}/\text{Fe}]$ ratios are shown in Figure 5. The observed ranges of Rb and Zr in low-mass and intermediate-mass AGB stars (shaded regions) in the Galaxy and Magellanic Clouds are also shown for comparison. The comparison shows clear evidence of consistency between observed abundances of Rb and Zr in the Ba stars and their counterparts normally observed in the low-mass AGB stars. The negative values of $[\text{Rb}/\text{Zr}]$ ratio obtained in the program stars confirm a low-mass companion for these stars.

4.2 Comparison with FRUITY models and a parametric-model-based analysis

The observed abundances in the atmosphere of the Ba stars might not be the actual signature of the progenitor AGB stars. The accreted s-process-rich material is mixed and diluted in the envelope of these secondary Ba stars. The diluted theoretical abundance on the surface of Ba stars is given as (Husti *et al.* 2009)

$$[\text{X}/\text{Fe}] = \log(10^{[\text{X}/\text{Fe}]^{\text{ini}}} \cdot f + 10^{[\text{X}/\text{Fe}]^{\text{AGB}}} \cdot 10^{-d}),$$

where d is the dilution factor, $f = 1 - 10^{-d}$ and $[\text{X}/\text{Fe}]^{\text{AGB}}$ the abundance of element X in the AGB. In this formulation it is assumed that both the AGB and the Ba stars are formed from the same cloud of interstellar medium (Husti *et al.* 2009).

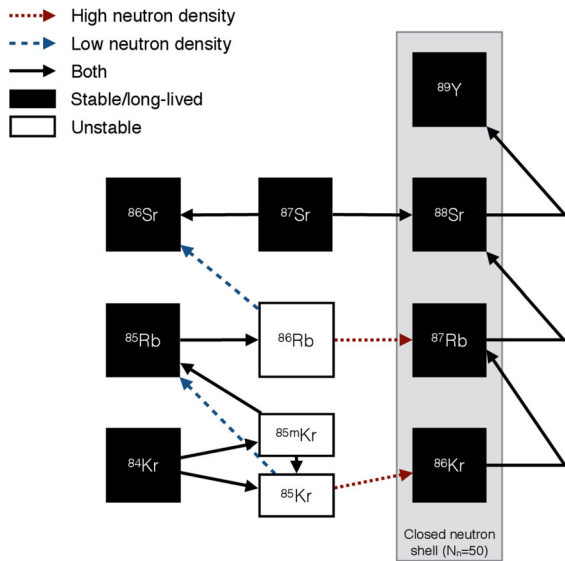


Figure 4. The s-process path from Kr to Zr. Stable isotopes are represented by a white box, while a black box represents the unstable ones. The solid arrows indicate s-process path branches specific to low neutron densities. The dashed arrows indicate s-process path branches followed under high neutron densities. The open rectangular box surrounds the isotopes with magic neutron number $N = 50$ (van Raai *et al.* 2012).

We have performed a parametric-model-based analysis to confirm the mass of the companion AGB stars by incorporating the dilution experienced by the s-process-rich material after the mass transfer. The dilution factor, d , is defined as $M_{\star}^{\text{env}}/M_{\text{AGB}}^{\text{transf}} = 10^d$, where M_{\star}^{env} is the mass of the envelope of the observed star after the mass transfer and $M_{\text{AGB}}^{\text{transf}}$ the mass transferred from the AGB. The dilution factor is derived by comparing the observed abundance with the predicted abundance from the FRUITY model for the heavy elements (Rb, Sr, Y, Zr, Ba, La, Ce, Pr, Nd, Sm and Eu). A publicly available (<http://fruity.oa-teramo.inaf.it/>), website of the Teramo Observatory (INAF)) data set for the s-process in AGB stars is the

FRANEC Repository of Updated Isotopic Tables & Yields (FRUITY) models (Cristallo *et al.* 2009, 2011, 2015). These models cover the whole range of metallicity observed for Ba stars from $z = 0.001$ to $z = 0.020$ for the mass range $1.3\text{--}6.0 M_{\odot}$. We have compared our estimated abundances with the FRUITY model. The solar values are taken as the initial composition. The observed elemental abundances are fitted with the parametric-model function. The best-fitting masses and corresponding dilution factors along with the χ^2 values are given in Table 2. A few examples of the best fits obtained are shown in Figure 6. All the Ba stars are found to have low-mass AGB companions with $M \leq 3 M_{\odot}$.

In FRUITY models where a standard ^{13}C pocket is considered, the different ^{13}C pocket efficiencies may explain the observed discrepancy. Also, inclusion of stellar rotations may cause the deviation in the observed abundance pattern, which is lacking in the current FRUITY models. Rotation-induced mixing is found to alter the extent of the ^{13}C pocket, altering the s-process abundance pattern (Langer *et al.* 1999). However, we note that a study by Cseh *et al.* (2018) using the rotating-star models available for the metallicity range of Ba stars (Piersanti *et al.* 2013) could not reproduce the observed abundance ratios of stars studied in de Castro *et al.* (2016).

4.3 The [hs/lr] ratio

In addition to the [Rb/Zr] ratio, the [hs/lr] ratio in Ba stars is an indicator of the neutron source and hence the mass of AGB stars. Here lr refers to the light s-process elements (Sr, Y and Zr) and hs to the heavy s-process elements (Ba, La, Ce and Nd). The observed [hs/lr] ratio is in the range 0.19–1.15, which agrees with the model calculations of Busso *et al.* (2001) for similar metallicities, for low-mass AGB stars

Table 1. Estimates of [Rb/Fe], [Zr/Fe] & [Rb/Zr].

Star name	[Fe/H]	[Rb/Fe] (± 0.20 dex)	[Zr/Fe] (± 0.20 dex)	[Rb/Zr] (± 0.20 dex)
HD 32712	-0.25 ± 0.12	-1.13	0.52	-1.65
HD 36650	-0.02 ± 0.12	-0.82	0.51	-1.33
HD 179832	$+0.23 \pm 0.04$	-1.35	1.29	-2.64
HD 211173	-0.17 ± 0.10	-1.00	0.38	-1.38

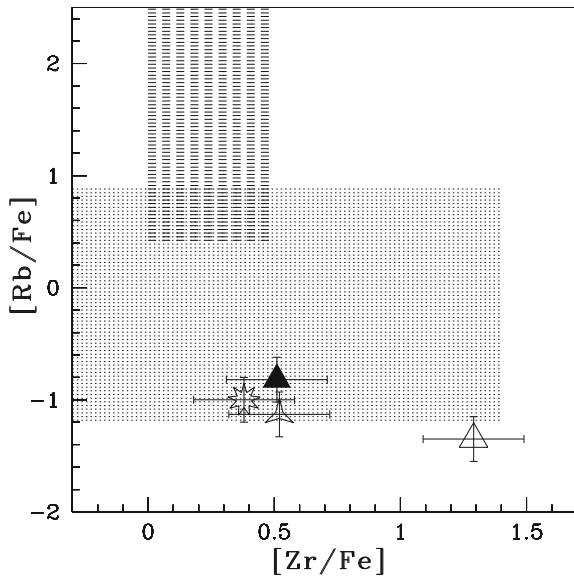


Figure 5. The observed abundances $[Rb/Fe]$ versus $[Zr/Fe]$ in HD 32712 (starred triangle), HD 36650 (filled triangle), HD 179832 (open triangle) and HD 211173 (nine-sided star). The regions shaded with short dashes and dots correspond to the observed range of Zr and Rb in intermediate-mass and low-mass AGB stars respectively in the Galaxy and the Magellanic Clouds (van Raai *et al.* 2012).

Table 2. The best-fitting mass, dilution factor and reduced chi-square values

Star name	M_{AGB} (M_{\odot})	d	χ^2
HD 32712	2.0	0.001	16.14
HD 36650	3.0	0.04	8.08
HD 179832	3.0	0.75	48.01
HD 211173	2.5	0.03	18.15

considering $^{13}C(\alpha, n)^{16}O$ neutron source. This also confirms the lower mass for the companion AGBs.

4.4 Comparison with low-mass AGB abundance

We have compared the observed abundance ratios for eight neutron-capture elements in the Ba stars with their counterparts in the low-mass AGB stars from the literature, that are found to be associated with $^{13}C(\alpha, n)^{16}O$ neutron source (Figure 7). The comparison shows a pretty good match between the abundances observed in both Ba stars and the AGBs. The

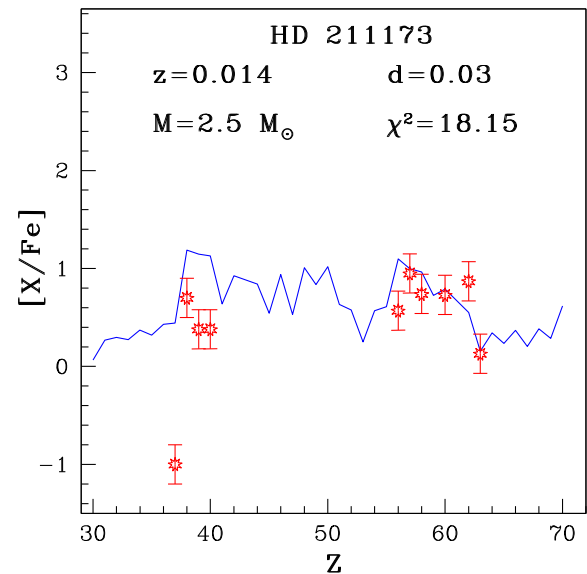
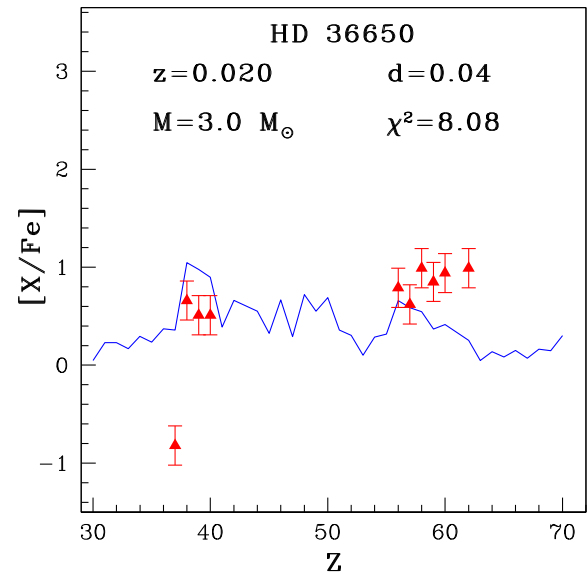


Figure 6. Observed elemental abundances and the parametric-model function. The solid curve represents the best fit for the parametric-model function. The points with error bars indicate the observed abundances in the program stars.

scatter observed in the ratios may be a consequence of different dilution factors during the mass transfer, as well as the orbital parameters, metallicity and initial mass (de Castro *et al.* 2016).

4.5 Mg abundance in support of neutron source

Another check for companion AGB mass is the Mg abundance. An Mg enrichment is expected to be observed in the stars if the s-process overabundance is resulting from the neutrons produced during the

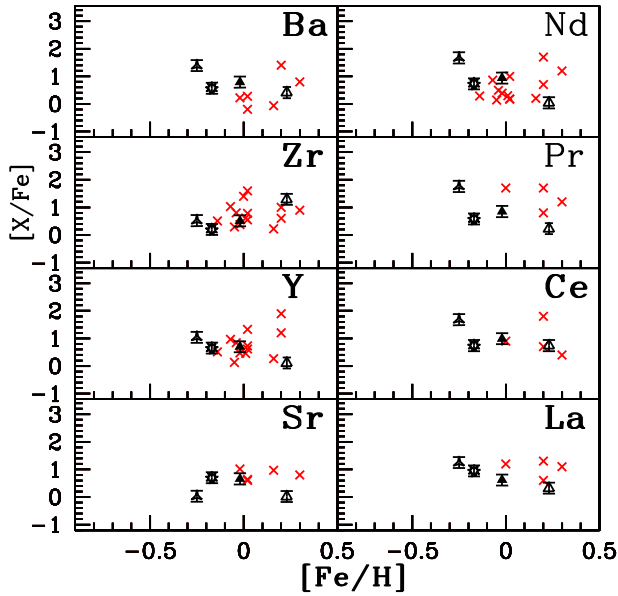


Figure 7. Comparison of abundance ratios of neutron-capture elements observed in the program stars and the AGB stars with respect to metallicity $[Fe/H]$. Red crosses represent AGB stars from the literature (Smith and Lambert 1985, 1986, 1990; Abia and Wallerstein 1998). Symbols: HD 32712 (starred triangle), HD 36650 (filled triangle), HD 179832 (open triangle), HD 211173 (nine-sided star).

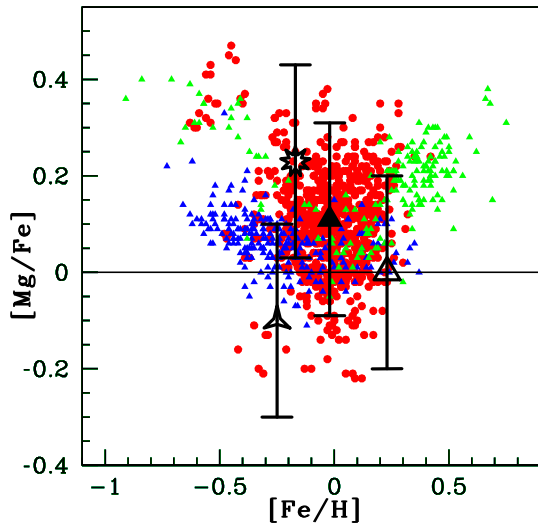


Figure 8. Abundances of Mg in our program stars, HD 32712 (starred triangle), HD 36650 (filled triangle), HD 179832 (open triangle) and HD 211173 (nine-sided star), compared with disk dwarfs and field giants. Red circles represent normal field giants from the literature (Luck and Heiter 2007), blue triangles represent thin disk dwarfs from Bensby *et al.* (2004) and Reddy *et al.* (2003), green triangles represent thick disk dwarfs from Bensby *et al.* (2004) and Reddy *et al.* (2006).

convective thermal pulses through the reaction $^{22}\text{Ne}(\alpha, n)^{25}\text{Mg}$. A comparison of the Mg abundances observed in the program stars and those in the disk stars and field giants is illustrated in Figure 8. As is obvious from the figure, we could not find any enhancement of Mg in our sample when compared to the disk stars and normal giants. This discards the possibility that the source of neutron is the $^{22}\text{Ne}(\alpha, n)^{25}\text{Mg}$ reaction.

5. Conclusion

The detection of Rb I line at 7800.259 \AA in the spectra of four program stars allowed us to determine $[Rb/Zr]$ ratio for these objects. The negative values obtained for this ratio in these stars indicate the operation of $^{13}\text{C}(\alpha, n)^{16}\text{O}$ reaction. As this reaction occurs in the low-mass AGB stars, we confirm that the former companions of these stars are low-mass AGB stars with $M \leq 3 M_{\odot}$. A comparison of observed abundances with the predictions from FRUITY models, and with those that are observed in low-mass AGB stars from the literature, also confirms low mass for the former companion AGB stars. The observed $[hs/l]$ ratio in the range 0.19–1.15, which agrees with the model calculations of Busso *et al.* (2001) for AGB stars considering $^{13}\text{C}(\alpha, n)^{16}\text{O}$ neutron source, is also an indication of low mass for the companion AGBs. An enhancement of Mg abundances compared to their counterparts in disk stars and normal giants would have indicated the operation of $^{22}\text{Ne}(\alpha, n)^{25}\text{Mg}$. We did not find any enhancement of Mg in our sample and hence discard the $^{22}\text{Ne}(\alpha, n)^{25}\text{Mg}$ reaction as the source of neutron. This again confirms low mass for the companion AGBs.

Acknowledgements

Funding from the DST SERB Project No. EMR/2016/005283 is gratefully acknowledged. This work made use of the SIMBAD astronomical database, operated at CDS, Strasbourg, France, and the NASA ADS, USA. This work has made use of data from the European Space Agency (ESA) mission Gaia (<https://www.cosmos.esa.int/gaia>), processed by the Gaia Data Processing and Analysis Consortium (DPAC, <https://www.cosmos.esa.int/web/gaia/dpac/consortium>).

References

- Abia C., Wallerstein G. 1998, *MNRAS*, 293, 89
- Abia C., Busso M., Gallino R., Domínguez I., Straniero O., Isern J. 2001, *ApJ*, 559, 1117
- Allen D.M., Barbuy B., 2006, *A&A*, 454, 895
- Barbuy B., Jorissen A., Rossi S. C. F. & Arnould M., 1992, *A&A*, 262, 216
- Beer H., 1991, *ApJ*, 375, 823
- Beer H. & Macklin R. L., 1989, *ApJ*, 339, 962
- Bensby T., Feltzing S., Lundstrom I., 2004, *A&A*, 415, 155
- Bidelman W.P., Keenan P.C., 1951, *ApJ*, 114, 473
- Busso M., Gallino R., Wasserburg G. J., 1999, *ARA&A*, 37, 239
- Busso M., Gallino R., Lambert D. L., Travaglio C., Smith V. V., 2001, *ApJ*, 557, 802
- Cristallo S., Straniero O., Gallino R., Piersanti L., Domínguez I., Lederer M. T., 2009, *ApJ*, 696, 797
- Cristallo S., Piersanti L., Straniero O., Gallino R., Domínguez I., Abia C., di rico G., Quintini M., Bisterzo S., 2011, *ApJS*, 197, 17
- Cristallo S., Straniero O., Piersanti L. & Gobrecht D., 2015, *ApJS*, 219, 40
- Cseh B., Lugaro M., D'Orazi V., de Castro D. B., Pereira C.B., Karakas A. I. et al., 2018, *A&A*, 620, A146
- de Castro D.B., Pereira C.B., Roig F., Jilinski E., Drake N.A., Chavero C., Sales Silva J.V., 2016, *MNRAS*, 459, 4299
- Drake N. A. & Pereira C. B., 2008, *AJ*, 135, 1070
- Gallino R., Arlandini C., Busso M., Lugaro M., Travaglio C., Straniero O., Chieffi A., Limongi M., 1998, *ApJ*, 497, 388
- García-Hernández D. A., García-Lario P., Plez B., D'Antona F., Manchado A., Trigo-Rodríguez M., 2006, *Science*, 314, 1751
- García-Hernández D. A., García-Lario P., Plez B., Manchado A., D'Antona F., Lub J. & Habing H., 2007, *A&A*, 462, 711
- García-Hernández D. A., Manchado A., Lambert D. L., Plez B., García-Lario P., D'Antona F., Lugaro M., Karakas A. I. & van Raai M. A., 2009, *ApJ*, 705, L31
- Goriely S., Mowlavi N., 2000, *A&A*, 362, 599
- Heil M., Käppeler F., Uberseder E., Gallino R., bisterzo S., Pignatari M., 2008, *Phys. Rev. C*, 78, 5802
- Husti L., Gallino R., Bisterzo S., Straniero O. & Cristallo S., 2009, *PASA*, 26, 176
- Iben Jr. I., 1975, *ApJ*, 196, 525
- Jonsell K., Barklem P. S., Gustafsson B., Christlieb N., Hill V., Beers T. C., Holmberg J., 2006, *A&A*, 451, 651
- Jorissen A., Boffin H. M. J., Karinkuzhi D., Van Eck S., Escorza A. et al., 2019, *A&A*, 626A, 127J
- Karakas A.I., García-Hernández D. A. & Lugaro M., 2012, *ApJ*, 751, 8
- Karinkuzhi D., Goswami A., Sridhar N., Masseron T., Purandardas M., 2018, *MNRAS*, 476, 3086K
- Lambert D. L., Luck R. E., 1976, *Obs.*, 96, 100L
- Lambert D. L., Smith V. V., Busso M., Gallino R., Straniero O., 1995, *ApJ*, 450, 302
- Langer N., Heger A., Wellstein S., Herwig F., 1999, *A&A*, 346, L37
- Lü P. K., 1991, *AJ*, 101, 2229
- Lucatello S., Tsangarides S., Beers T. C., Carretta E., Gratton R. G., Ryan S. G., 2005, *ApJ*, 652, 825
- Luck R. E., Heiter U., 2007, *AJ*, 133, 2464
- Lugaro M., Chieffi A., 2011, in *Lecture Notes in Physics*, ed. R. Diehl, D. H. Hartmann & N. Prantzos (Berlin: Springer Verlag), 812, 83
- Mahanta U., Karinkuzhi D., Goswami A., Duorah K., 2016, *MNRAS*, 463, 1213
- McClure R. D., 1983, *ApJ*, 208, 264
- McClure R. D., 1984, *ApJ*, 280, 31
- McClure R. D., Woodsworth W., 1990, *ApJ*, 352, 709
- McClure R. D., Fletcher J. M., Nemeč J., 1980, *ApJ*, 238, L35
- McWilliam A., 1998, *AJ*, 115, 1640
- Pereira C. B., Drake N. A., 2009, *A&A*, 496, 791
- Piersanti L., Cristallo S., Straniero O., 2013, *ApJ*, 774, 98
- Plez B., Smith V. V. & Lambert D. L., 1993, *ApJ*, 418, 812
- Purandardas M., Goswami A., Goswami P. P., Shejeelammal J., Masseron T., 2019, *MNRAS*, 486, 3266
- Reddy B. E., Tomkin J., Lambert D. L. & Allende Prieto C., 2003, *MNRAS*, 340, 304
- Reddy B. E., Lambert D. L., Prieto C. A., 2006, *MNRAS*, 367, 1329
- Shejeelammal J., Goswami A., Goswami P. P., Rathour R. S., Masseron T., 2020, *MNRAS*, 492, 3708
- Smiljanic R., Porto de Mello G. F., da Silva L., 2007, *A&A*, 468, 679
- Smith V. V., Lambert D. L., 1985, *ApJ*, 294, 326
- Smith V. V., Lambert D. L., 1986, *ApJ*, 311, 843
- Smith V. V., Lambert D. L., 1990, *ApJS*, 72, 387
- Snedden C., 1973, PhD thesis, Univ. Texas
- Straniero O., Gallino R., Busso M., Chieffi A., Raiteri C. M., Limongi M., Salaris M., 1995, *ApJ*, 440, L85
- Tomkin J., Lambert D. L., 1983, *ApJ*, 273, 722
- Tomkin J., Lambert D. L., 1999, *ApJ*, 523, 234
- Udry S., Jorissen A., Mayor M., Van Eck S., 1998a, *A&AS*, 131, 25
- Udry S., Mayor M., Van Eck S., Jorissen A., Prévot L., Grenier S., Lindgren H., 1998b, *A&AS*, 131, 43
- van Raai M. A., Lugaro M., Karakas A. I., García-Hernández D. A., Yong D., 2012, *A&A*, 540, A44
- Worely C. C., Hill V. J., Sobeck J., Carretta E., 2013, *A&A*, 553, A47
- Yang G. C., Liang Y. C., Spite M., Chen Y. Q., Zhao G. et al., 2016, *RAA*, 16, 1